Coupling non-thermal plasma with V_2O_5/TiO_2 nanofiber catalysts for enhanced oxidation of ethyl acetate

Jinfei Wu [1], Xinbo Zhu [1,2,3,*], Yuxiang Cai [2], Xin Tu [3,*]

[1] Faculty of Maritime and Transportation, Ningbo University, Ningbo, 315211, P.R. China

[2] State Key Laboratory of Clean Energy Utilization, Zhejiang University, Hangzhou, 310027, P.R. China

[3] Department of Electrical Engineering and Electronics, University of Liverpool, Liverpool, L69 3GJ, UK

Corresponding Authors

Dr. Xinbo Zhu

Faculty of Maritime and Transportation

Ningbo University

Ningbo 315211

P.R. China

E-mail: zhuxinbo@nbu.edu.cn

Dr. Xin Tu

Department of Electrical Engineering and Electronics,

University of Liverpool,

Liverpool L69 3GJ

UK

E-mail: xin.tu@liverpool.ac.uk

Abstract

Plasma-catalytic oxidation of ethyl acetate was conducted in a dielectric barrier discharge (DBD) reactor. The effect of novel nanofiber catalysts (nano-V_5Ti and nano-TiO_2) and corresponding bulk catalysts on the plasma-catalytic process was investigated and compared with using plasma alone. The combination of plasma and nano-V_5Ti catalyst significantly showed the best plasma-catalytic oxidation performance. Catalyst characterization showed that nano-V_5Ti possessed smaller crystalline size and higher relative concentration of surface adsorbed oxygen (O_{ads}) species compared to the bulk catalysts, which played a key role in the enhanced oxidation of ethyl acetate and its intermediates on the catalyst surfaces. Compared to the bulk catalysts, the formation of more reduced vanadium species (V^{4+}) in the nano-V_5Ti catalysts indicated the presence of more oxygen vacancies on the nano-V_5Ti surface, which in turn improved the reducibility of nano-V_5Ti and facilitated surface oxygen species activation in the plasma region and contributed to the plasma-catalytic oxidation reactions.

Keywords: Plasma-catalysis; Non-thermal plasma; VOC oxidation; Vanadium oxide; Nano-catalyst

1. Introduction

The emission of volatile organic compounds (VOCs) has received significant attention, especially in developing countries, due to the negative effects of VOCs on both environment and human health since VOCs are one of the major precursors for the formation of haze and smog [1]. Ethyl acetate, one of the most stable VOC molecules, was employed as the model pollutant in this work, since it's widely used as a solvent in various industrial processes including printing operation, nail polish removers and glues, etc.. Plasma-catalytic process has been regarded as a promising and cost-effective technology for the purification of low concentration gas pollutants in large volume gas streams. A wide range of chemically reactive

species and energetic electrons can be generated by non-thermal plasmas even at room temperature. These reactive species and electrons are capable of breaking most chemical bonds or initiating chemical reactions with the pollutants, which consequently benefit the further oxidation of organic fragments to final products such as CO_2 and H_2O [2]. Bo et al. reported the oxidation of 91.4% ethyl acetate (1000 ppm) at the flow rate of 12 $L \cdot min^{-1}$ in a gliding arc reactor. However, the generation of over 5700 ppm NO_2 limited further application of this technology in gas purification [3]. Catalysts play a crucial role in determining the reaction performance. The presence of catalysts in the plasma process has great potential to generate a synergistic effect resulting from the interactions between the plasma and catalysts, which can significantly enhance the removal efficiency of pollutants and energy efficiency of the plasma-catalytic process. The combination of plasma with the catalysts can overcome the low selectivity of the plasma process and drive the reactions towards the desired direction of deep oxidation and minimize the formation of unwanted byproducts [4-6].

Up until now, a series of rare earth catalysts have been developed for VOC oxidation [7-9]. Tsoncheva et al. compared the effect of a series of cobalt oxides supported by different mesoporous silicas on ethyl acetate oxidation, while the Co/KIT-6 catalyst showed ~100% conversion rate around 600K [10]. Gandhe et al. developed a highly efficient OMS-2 based catalyst for the oxidation of ethyl acetate with 100% conversion (625K) and selectivity to CO_2 (675K) [11]. Among the potential catalysts, vanadium-based catalysts have been intensively investigated in thermal-catalytic oxidation of various pollutants including hydrocarbons [12], aromatics [13-14], organic sulfide [15-16] and dioxins [17-18] due to their comparative activity, relative low cost and good resistance to poisonings compared to noble metal catalysts [19]. However, very limited efforts have been devoted to the investigation of plasma-catalytic oxidation of gas pollutants using these catalysts [20-23]. In our previous study, we also found that the combination of a dielectric barrier discharge (DBD) plasma with V-W/Ti catalysts enhanced the removal of

dimethyl sulfide and energy efficiency of the plasma-catalytic process [24]. However, the performance of the bulk vanadia-based catalysts still needed to be improved to make the plasma-catalytic oxidation process more attractive. In addition, the knowledge of vanadia-based catalysts for the plasma-catalytic oxidation of VOCs is rather limited, while the synergy from the combination of non-thermal plasma with these catalysts is not clear, especially when a catalyst is placed in the plasma discharge.

Recently, nanomaterials have shown great potentials in heterogeneous catalysis for gas clean-up with outstanding catalytic properties compared to bulk catalysts considering their unique physical and chemical properties including the particle size, morphology and surface area, etc. [25-27]. Yu et al. reported that the removal efficiency and destruction efficiency of PCDD/Fs reached 96.7% and 75.0% at a reaction temperature of 200 °C when using a 5 wt.% V_2O_5/nano-TiO_2 catalyst, while the values were decreased to only 92.6% and 46.7% for a bulk 5 w.t.% V_2O_5/TiO_2 catalyst [18]. Bianchi et al. compared the activity of micro and nano-sized TiO_2 catalysts on photocatalytic degradation of gaseous acetone and found that the total oxidation of acetone was achieved in 70 min using the nano-sized TiO_2 catalyst while it took much longer (90 min) to obtain the total oxidation of acetone over the micro-sized TiO_2 catalyst [28]. More recently, Mok et al. reported that the shape of ZnO nanomaterials had significant effect on plasma-catalytic oxidation of butane, while the ZnO nanowire coated catalyst showed better removal efficiency and carbon balance compared to ZnO nanoparticle and nanorod [29]. However, to the best of our knowledge, there is very limited work focused on the combination of plasma with nano-catalysts for the removal of gas pollutants in plasma-catalytic processes [30-31]. In a plasma-catalytic system using nanomaterials as catalyst, the generation of discharge streamer, the mass transfer process and interactions between catalytic active sites and chemically reactive species/radicals could be quite different from those using bulk catalysts. The underlying mechanisms in plasma-nanomaterial system were

still far from clear [32-33].

In this work, novel V_2O_5/TiO_2 nanofiber and pure TiO_2 nanofiber catalysts were synthesized using a combined electrospinning and hydrothermal method. The effect of nanofiber catalysts (V_2O_5/TiO_2 and TiO_2) and bulk catalysts on the plasma-catalytic oxidation of low concentration ethyl acetate was investigated in a coaxial DBD reactor. The roles of the nano-catalysts in the plasma-catalytic oxidation process were examined by using a wide range of analytic techniques such as N_2 adsorption-desorption, X-ray diffraction (XRD), transmission and scanning electron microscopy (TEM and SEM), temperature programmed reduction with H_2 (H_2-TPR) and X-ray photoelectron spectroscopy (XPS). The possible reaction mechanisms involved in the plasma-catalytic oxidation process were also discussed.

2. Experimental section

2.1 Preparation of nanofibers

The V_2O_5/TiO_2 nanofiber catalysts were prepared by a combined electrospinning and hydrothermal methods involving the following two steps: (1) electrospinning of the precursor solution to obtain TiO_2 nanofibers; (2) hydrothermal growth of V_2O_5 nanoparticles on TiO_2 nanofibers to obtain hierarchical V_2O_5/TiO_2 nanofiber catalysts [34].

Firstly, desired amounts of polyvinylpyrrolidone (PvP, M_w=1,300,000), acetic acid and ethanol were mixed and vigorously stirred for 1 h. Then weighted amount of tetrabutyl titanate was added to the mixture and stirred overnight at room temperature to obtain viscous gel. The gel was electrospun at an applied voltage of 15 kV, while the injection speed and rotating speed of the collector were kept at 1 ml·h^{-1} and 50 rpm, respectively. The prepared samples were calcined at 500 °C for 5 h in a muffle to get the TiO_2 nanofibers (nano-TiO_2).

The growth of V_2O_5 nanoparticles on the TiO_2 nanofibers were carried out using the hydrothermal method. Appropriate amount of vanadium (III) acetylacetonate and urea were

dissolved and mixed in deionized water. Consequently, weighted hexadecyl trimethyl ammonium bromide (CTAB) and 0.5 ml polyethylene glycol (PEG, M_w=400) were added dropwisely into the mixed solution under vigorous stirring. Then, the samples were impregnated on the TiO_2 nanofibers in a Teflon autoclave. The hydrothermal temperature was kept at 120 °C for 24 h to get the white film. The film was repeatedly washed with an ethanol-water mixture and dried under vacuum at 50 °C overnight. Finally, the samples were calcined at 400 °C for 5h and sieved to 35-60 meshes. In this work, the loading amount of V_2O_5 on TiO_2 nanofibers were 5 wt.% (denoted as nano-V_5Ti). Bulk V_2O_5/TiO_2 (denoted as bulk-V_5Ti) with the same vanadium loading (5 wt.%) and pure TiO_2 catalysts were prepared using conventional impregnation method for comparison.

2.2 Catalyst characterization

The morphology of catalyst samples was observed with thermal field-emission scanning electron microscopy (FE-SEM) with a SIRION-100 microscope. High-resolution transmission electron microscopy (HRTEM) was conducted on a Tecnai F20 microscope operating at an acceleration voltage of 200 kV.

N_2 adsorption-desorption experiments were carried out using a Quantachrome Autosorb-1 instrument at -196 °C to obtain the structural properties of the V_2O_5/TiO_2 and TiO_2 catalysts including the specific surface area, average pore size and pore volume.

The X-ray diffraction (XRD) patterns of the catalysts were recorded by a Rikagu D/max-2000 X-ray system equipped with a Cu-Ka radiation source. The scan range was from 10° to 80° with a scanning step size of 0.02°.

X-ray photoelectron spectroscopy (XPS) spectra were performed with a Thermo ESCALAB 250 using Al Kα X-ray (hν = 1486.6 eV) at a constant pass energy of 1486.6 eV as the radiation source. The binding energies of V 2p, Ti 2p and O 1s were calibrated with the C 1s

binding energy (B. E.) value of 284.6 eV.

The reducibility of the catalysts was determined by temperature-programmed reduction with hydrogen (H_2-TPR) using a chemisorption analyzer (Micrometrics, Autochem II 2920). Each catalyst (30 mg) was pretreated in a nitrogen flow for 1 h at 200 °C before the test. The catalyst samples were consequently heated from room temperature to 800 °C at a heating rate of 10 °C min^{-1} in a 10% H_2/Ar flow with a total flow rate of 40 ml·min^{-1}.

2.3 Experimental setup

The experiment setup of the plasma-catalytic system (**Figure 1**) was described in detail elsewhere [35]. A 60 mm-long aluminum foil was wrapped tightly around a quartz tube (i.d.=8 mm, o.d.=10 mm) as a ground electrode. A stainless-steel rod (ϕ = 4 mm) was placed in the axis of the quartz tube and acted as a high voltage electrode. Gaseous ethyl acetate was generated from a gas cylinder (0.1% ethyl acetate, balanced air), while zero grade air was used as a carrier gas in this work. All gas streams were premixed before introduced into the DBD reactor. In this work, the inlet concentration of ethyl acetate was 100 ppm and the total flow rate was fixed at 1 L·min^{-1}. For each experiment, 200 mg catalysts were packed into the discharge area and held by quartz wool, resulted in a gas hourly space velocity (GHSV) of 300000 mL·g^{-1}·h^{-1}. The temperature of the outer surface of the DBD reactor was measured below 85 °C.

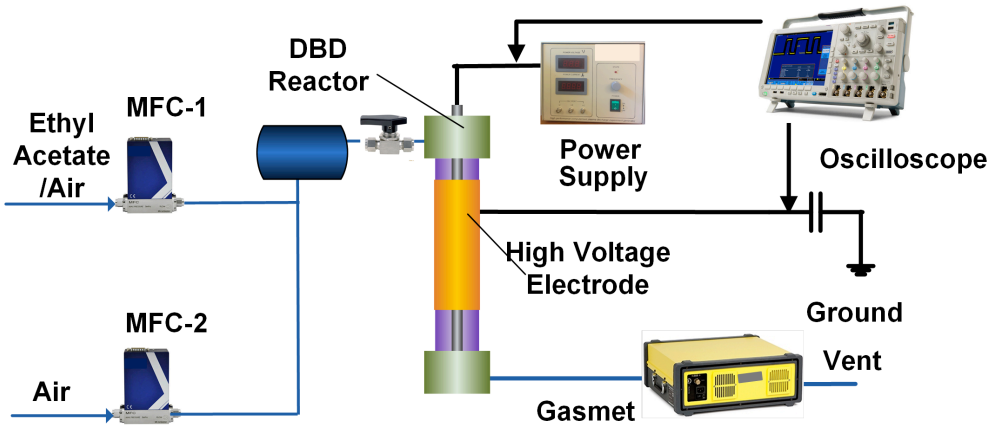

Figure 1. Schematic diagram of experimental setup.

The DBD reactor was connected to a high voltage power supply (CTP-2000, Suman) with a maximum peak voltage of 30 kV. The discharge frequency was fixed at 10 kHz in this study. The applied voltage was measured by a 1000:1 voltage probe (Tektronix P6015A), while the voltage over the external capacitor (0.47 μF) was monitored by a passive probe (Tektronix TPP0500). All the electrical signals were recorded using a digital oscilloscope (Tektronix 4034B). The discharge power was calculated based on the Q-U Lissajous method. The specific energy density (SED) was defined as:

$$SED\ (J \cdot L^{-1}) = \frac{P\ (W)}{Q\ (L \cdot min^{-1})} \times 60 \tag{1}$$

where P is the discharge power and Q is the total flow rate.

Gas compositions were measured online using a calibrated multi-component gas analyzer (Gasmet Dx4000, Finland). The instrument was equipped with a 0.4 L gas cell with an effective path length of 5 m. All the measurements were carried out after running the plasma-catalytic reaction for 45 min when a steady-state of the process was reached and repeated 3 times. The removal efficiency ($\eta_{\text{ethyl acetate}}$), CO_2 selectivity and carbon balance of plasma-catalytic oxidation of ethyl acetate was defined as:

$$\eta_{\text{ethyl acetate}} = \frac{c_{in} - c_{out}}{c_{in}} \times 100\% \tag{2}$$

$$CO_2\ selectivity(\%) = \frac{c_{co_2}}{4 \times (c_{in} - c_{out})} \times 100\% \tag{3}$$

$$Carbon\ Balance(\%) = \frac{c_{co_2} + c_{co} + 4 \times c_{out}}{4 \times c_{in}} \times 100\% \tag{4}$$

where c_{in} and c_{out} are the inlet and outlet concentrations of ethyl acetate, respectively. c_{co} and c_{co_2} are CO and CO_2 concentrations in the effluent, respectively.

3. Results and Discussions

3.1 Characterization of nanofiber catalysts

Figure 2 shows the SEM images of the as-prepared nanofiber and bulk catalyst samples. The nano-V_5Ti and nano-TiO_2 catalysts had well-defined one-dimensional morphology and the nanofibers intertwine to form compact networks, as shown in **Figure 2(a)** and **(b)**. The average diameter of pure nano-TiO_2 fibers was around 550 nm, while the doping of vanadium species on nano-TiO_2 fibers slightly increased the average diameter of the nanofibers to ca. 590 nm. The micro-morphology of all the catalysts was further analyzed by HRTEM (**Figure 3**), while the inner-planar spacing of the samples was also presented. The lattice fringes for both nano-TiO_2 and bulk-TiO_2 were 3.52 Å, indicating the presence of the (101) crystal face of anatase TiO_2 (JCPDS 21-1272). The lattice fringes of 3.52 Å and 3.49 Å showed up in the nano-V_5Ti and bulk-V_5Ti catalysts. The latter one corresponded to the (111) crystal face of monoclinic V_2O_5 (JCPDS 54-0513). These results confirmed the existence of vanadium species on the TiO_2 nanofiber support.

The isotherms of the N_2 adsorption-desorption for the nanofiber catalysts were of type IV, which corresponded to the capillary condensation of the adsorbents inside the mesopores of the nanofibers. Type H3 hysteresis loops were also observed in the nanofiber catalysts, indicating the existence of open slit-shaped pores with parallel walls as classified by IUPAC [36]. **Table 1** gives the specific surface area (S_{BET}) and average pore volume of the catalysts. The S_{BET} of the nano-TiO_2 and bulk-TiO_2 samples were 42.2 $m^2 \cdot g^{-1}$ and 48.0 $m^2 \cdot g^{-1}$, respectively. The addition of vanadium species onto nano-TiO_2 fibers significantly reduced the S_{BET} of the nano-TiO_2 to 14.9 $m^2 \cdot g^{-1}$ for the nano-V_5Ti catalyst. In contrast, for the bulk catalysts, vanadium doping only slightly decreased the S_{BET} of the bulk V_5Ti catalyst to 41.5 $m^2 \cdot g^{-1}$ compared to that of the bulk-TiO_2. Similar observation was found in the average pore volume of the catalysts, which was reduced by 64.2% for the nanocatalysts and 5.4% for the bulk catalyst after vanadium

doping. This phenomenon could be ascribed to the blockage of micro-pores of the catalyst supports and the coverage of catalyst surfaces by vanadium species [37].

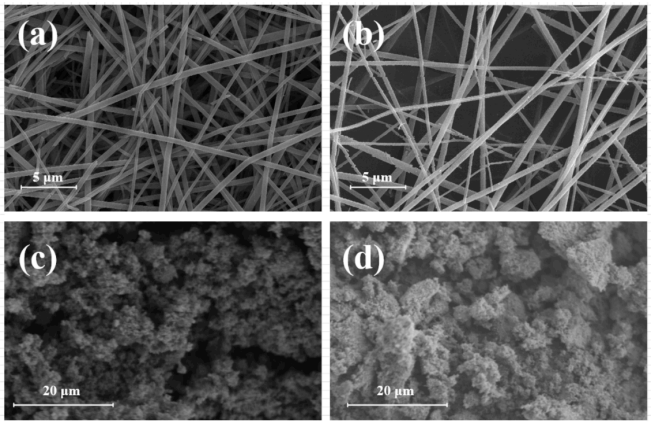

Figure 2. SEM images of the catalysts: (a) nano-V_5Ti, (b) nano-TiO_2, (c) bulk-V_5Ti, (d) bulk-TiO_2.

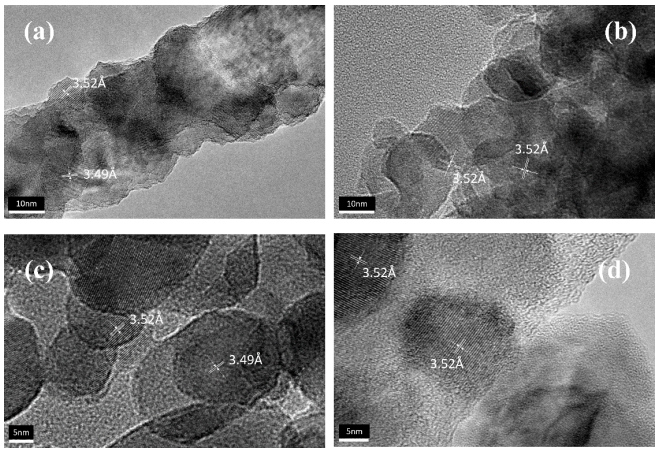

Figure 3. HRTEM images of the catalysts: (a) nano-V_5Ti, (b) nano-TiO_2, (c) bulk-V_5Ti, (d) bulk-TiO_2.

In **Figure 4**, the XRD patterns of all the catalysts showed major diffraction peaks centered at 2θ= 25.3°, 37.8°, 48.0°, 53.9° and 55.1°, which were well associated with the crystal faces of (101), (004), (200), (105) and (211) of the tetragonal anatase TiO_2 (JCPDS 21-1272). In addition, the presences of weak diffraction peaks of rutile TiO_2 at 2θ=27.4° in all samples corresponds to the (110) crystal face. No significant changes in the crystalline structure of the

catalysts were observed when doping 5 wt.% vanadium species on TiO_2. The diffraction peaks of all V_5Ti catalysts were broader compared to those of pure TiO_2 supports, which is in accordance with the crystalline sizes calculated using the Scherrer's equation (**Table 1**). Moreover, the crystalline size of the nanofiber catalysts was about 30% smaller compared to that of the bulk catalysts, i.e. 14.88 nm for nano-V_5Ti and 20.73 nm for bulk-V_5Ti, respectively.

Table 1. Physico-chemical properties of the catalysts.

Sample	S_{BET} ($m^2 \cdot g^{-1}$)	Average pore volume ($cm^3 \cdot g^{-1}$)	Crystalline size (nm)[a]	$V^{4+}/(V^{4+}+V^{5+})$ (%)	$O_{ads}/(O_{ads}+O_{lat})$ (%)
Nano-V_5Ti	14.9	0.05	14.88	30.3	15.4
Nano-TiO_2	42.2	0.14	15.45	n.a.	13.3
Bulk-V_5Ti	41.5	0.35	20.73	22.8	13.6
Bulk-TiO_2	48.0	0.37	22.34	n.a.	10.5

[a] Calculated from the (101) crystal face of anatase TiO_2 at 2θ =25.3°.

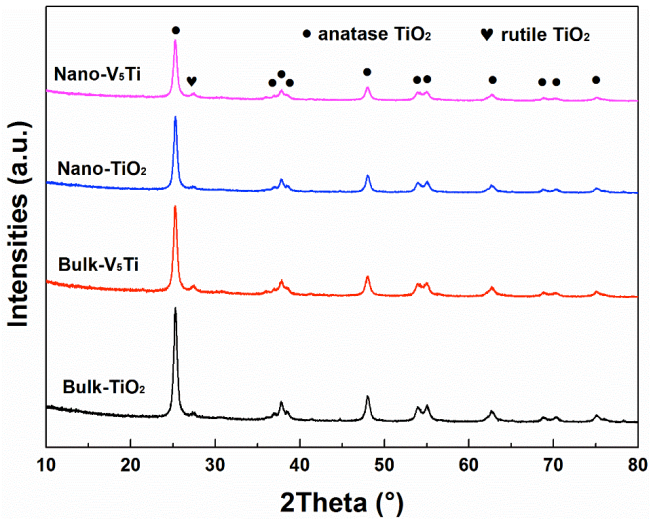

Figure 4. XRD patterns of the catalysts.

XPS analysis was used to get insights of the chemical states of the elements in the catalysts. **Figure 5(a)** shows the XPS spectra of O 1s for all four catalysts. Two major peaks can be obtained by fitting the curves. The peaks located at 529.6-530.0 eV can be attributed to the formation of lattice oxygen (O^{2-}) (denoted as O_{lat}) on the catalyst surface, while those peaks located between 531.4 eV and 532.1 eV could be ascribed to the production of

surface-adsorbed oxygen (denoted as O_{ads}). The relative concentration of O_{ads}, for each catalyst, defined as $O_{ads}/(O_{ads}+O_{lat})$, was calculated based on the XPS spectra (Table 1). The value of $O_{ads}/(O_{ads}+O_{lat})$ of all the catalysts varied from 10.5% to 15.4%, while the nano-V_5Ti catalyst had the highest relative concentration of O_{ads}.

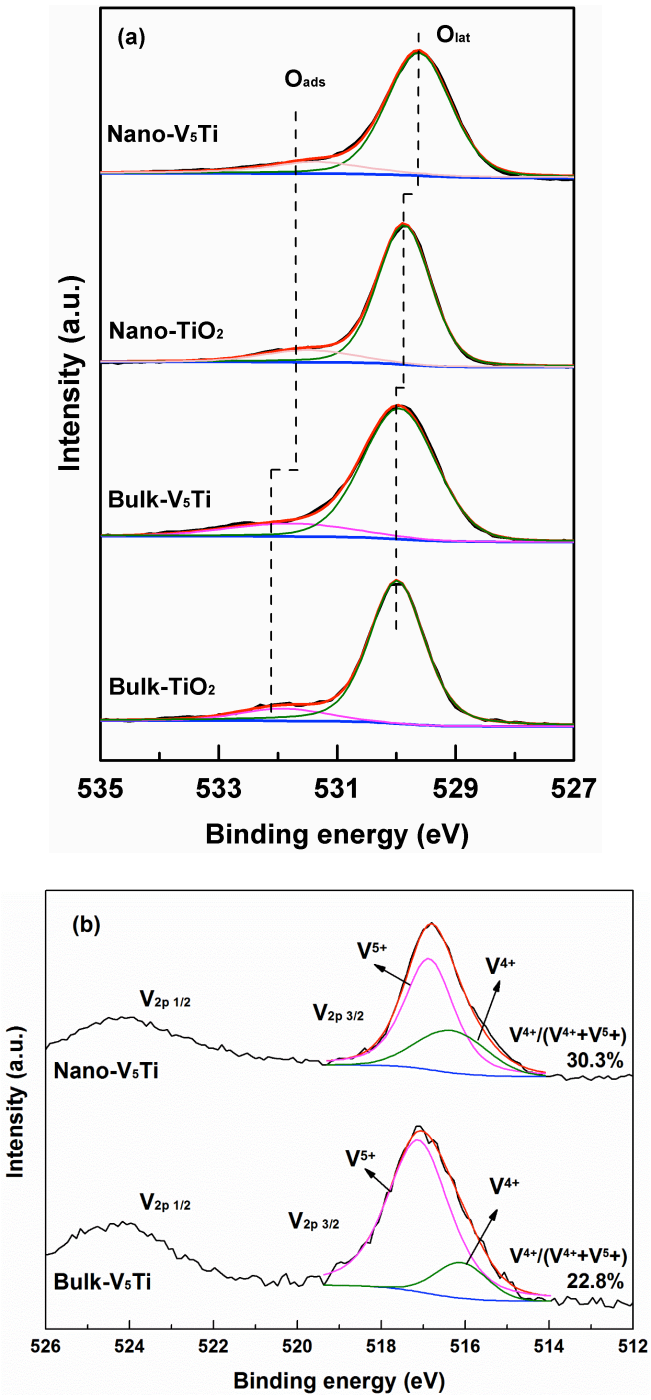

Figure 5. XPS spectra of the V_5Ti catalysts: (a) O 1s, (b) V 2p.

Figure 5(b) shows the XPS results of V 2p of the nano-V_5Ti and bulk-V_5Ti catalysts. For both samples, the XPS profiles of V 2p show two major peaks at around 524 eV and 517 eV, which belong to V $2p_{1/2}$ and V $2p_{3/2}$, respectively. The asymmetric spectra of V $2p_{3/2}$ indicate the existence of two types of vanadium species on the surface of the V_5Ti catalysts. The deconvolution of the V $2p_{3/2}$ for the V_5Ti catalysts exhibits two peaks centered at 517.2 eV and 516.3 eV. The former peak can be identified as V^{5+}, while the latter one belongs to V^{4+}. The relative concentration of V^{4+}, defined as $V^{4+}/(V^{4+}+V^{5+})$, was 30.3% for the nano-V_5Ti catalyst and 22.8% for the bulk-V_5Ti catalyst.

H_2-TPR experiment was carried out to evaluate the reducibility of both bulk and nano-sized V_5Ti catalysts (**Figure 6**). The results of pure TiO_2 samples were not presented since only very weak signals were observed around the reduction temperature of 640 °C and 650 °C for the nano-TiO_2 and bulk-TiO_2 catalysts, respectively. Similar observation was reported by Liu [38]. Two major reduction peaks could be observed in the reduction profile of both V_5Ti catalysts. The first peak could be attributed to the reduction of V^{5+} to V^{4+}, while the second one was related to the conversion of Ti^{4+} to Ti^{3+}. Compared to the bulk-V_5Ti catalyst, the first reduction peak of the V_5Ti nanofiber catalyst shifted from 406 °C to 359 °C, while the second reduction peak of the V_5Ti nanofiber catalyst slightly moved from 601 °C to 589 °C [39].

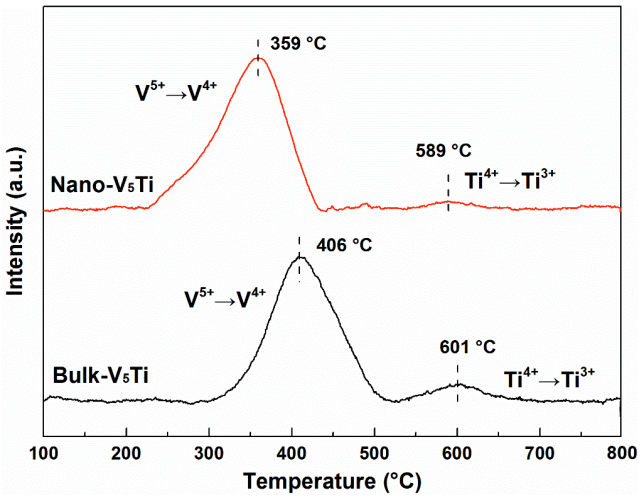

Figure 6. H_2-TPR profiles of the V_5Ti catalysts.

3.2 Performance of plasma-catalysis

Figure 7 shows the effect of different catalysts on the plasma-catalytic oxidation of ethyl acetate in terms of the removal efficiency as a function of SED. Clearly, the removal efficiency of ethyl acetate increased almost monotonically with increasing the SED, regardless of the presence of catalysts or the catalyst type. For example, in the case of using plasma alone, the ethyl acetate removal efficiency increases from 10.6% to 51.5% over the SED range of 304.8 $J \cdot L^{-1}$ to 604.8 $J \cdot L^{-1}$. Similarly, in the plasma-catalysis system, increasing the SED from 302.4 $J \cdot L^{-1}$ to 596.4 $J \cdot L^{-1}$ significantly enhanced the removal efficiency of ethyl acetate by a factor of ~6 (from 10.9% to 65.8%) in the plasma reaction combined with the bulk-TiO_2 catalyst. Similarly, the removal efficiency of ethyl acetate increased from 10.2% to 80.7% with the increase of the SED from 279.6 $J \cdot L^{-1}$ to 573.6 $J \cdot L^{-1}$ when the nano-TiO_2 catalyst was placed in the plasma reactor. The removal efficiency of ethyl acetate in the plasma-catalytic process at the same SED follows the order of nano-V_5Ti > bulk-V_5Ti > nano-TiO_2 > bulk-TiO_2, while the highest removal efficiency of 99.0% was obtained at a SED of 579.6 $J \cdot L^{-1}$ using the nano-V_5Ti catalyst. The effects of different catalysts on carbon balance and CO_2 selectivity in the plasma-catalytic oxidation of ethyl acetate are presented in **Figure 8**. The variation of the carbon balance and CO_2 selectivity as a function of SED followed the similar trends as the removal efficiency of ethyl acetate. The carbon balance and CO_2 selectivity increase from 74.9% to 87.4% and 36.2% to 45.1% in the SED range of 304.8 $J \cdot L^{-1}$ to 604.8 $J \cdot L^{-1}$. The presence of heterogeneous catalysts significantly improve the carbon balance and CO_2 selectivity of the plasma-catalytic oxidation process for ethyl acetate oxidation. Among the employed catalysts, the bulk-TiO_2 catalyst showed the lowest carbon balance of 78.1% to 98.0% and CO_2 selectivity of 37.6% to 50.4% in the tested SED range followed by the nano-TiO_2, bulk-V_5Ti and nano-V_5Ti catalysts. The highest carbon balance of 99.3% and CO_2

selectivity of 55.6% were achieved in the presence of the nano-V_5Ti catalyst at the SED of 579.6 $J \cdot L^{-1}$. It is worth noting that the combination of the plasma with these nanofiber catalysts showed enhanced process performance compared to that using bulk catalysts under the same operating conditions, whilst the performance of plasma oxidation process using the vanadium doped catalysts was much higher than that using pure TiO_2 catalysts.

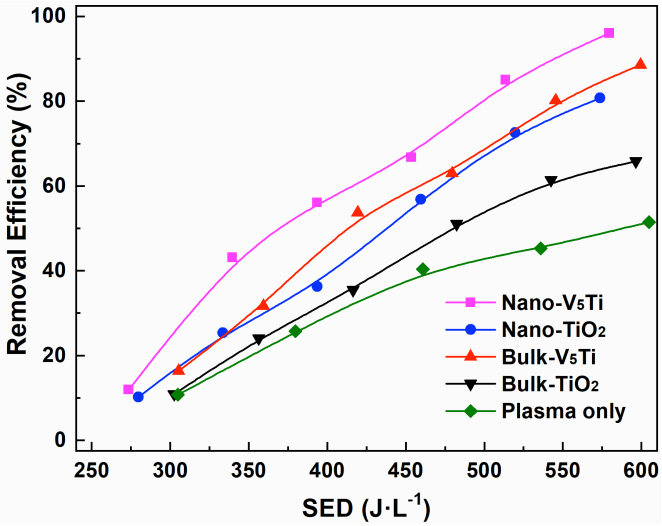

Figure 7. Effect of catalysts on plasma-catalytic oxidation of ethyl acetate.

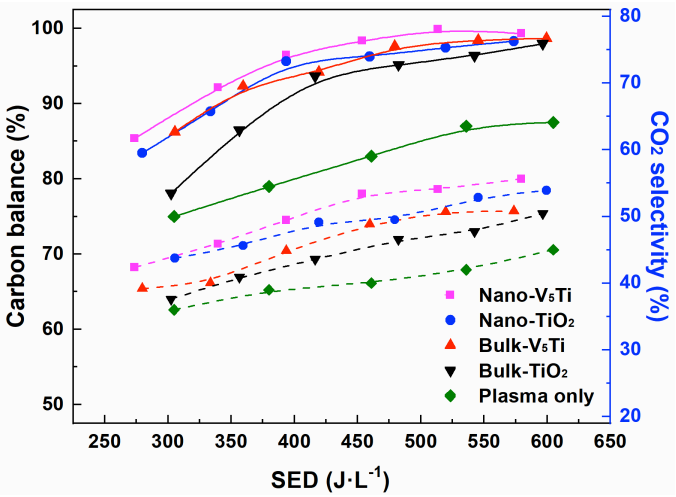

Figure 8. Effect of catalysts on carbon balance and CO_2 selectivity of plasma-catalytic oxidation of ethyl acetate.

3.3 Discussions

It is well accepted that air discharge generated by a coaxial DBD consists of numerous micro-discharge filaments which are randomly distributed in the discharge. More

micro-discharge filaments are expected to be generated near the contact regions between the catalyst pellets and the pellet-wall due to the intensified electric fields. These filaments are initiated by gas breakdowns and then become streamers propagating in the void or over the catalyst surface between the electrode and dielectric material [40]. Energetic electrons generated in the filaments are regarded as a driving force to initiate plasma chemical reactions. In this work, the energetic electrons collide with carrier gas (i.e. air) and ethyl acetate, generating numerous chemically reactive radicals including O, O(1D), N and metastable N_2, as well as the intermediates (organic fragments) from ethyl acetate. It is widely recognized that the C=O bond in VOC molecules is much stable compared to the C-O, C-H and C-C bonds [41]. Theoretically, the rupture of C-O, C-H and C-C chemical bonds were likely to occur by the direct bombard of energetic electrons considering their number densities and bond energies since the electron energy of the plasma was usually in the range of 1-10 eV. Previous studies of reaction kinetics in plug flow reactors reported the dissociations of C-O bonds were favoured over the cleverages of C-H and C-C bonds in ester molecules, while the oxidation of the C-H and C-C bonds cannot be ignored [42-43]. Similarly, once operated in air plasma region, ethyl acetate molecules would undergo a series of plasma-chemical reactions with the aid of highly chemically reactive species. The rupture of C-O bonds would generate $CH_3CO\cdot$ and $CH_3CH_2O\cdot$ radicals. There two radicals could be impacted by energetic electrons and reactive radicals (O and N radicals with sufficient energy) to small fragments including $CH_3\cdot$, $CH_2O\cdot$, $CH_3CH_2\cdot$ and CO, etc., while further oxidation of these species by O and $OH\cdot$ towards CH_3COOH and CH_3CH_3OH could also be expected. The small fragments could also be generated from the rupture of C-H and C-C bonds. Further H-abstraction occurs to generate $CH_x\cdot$ (x=1 and 2) radicals. All the aforementioned small fragments and radicals could be further oxidized and converted into the final products such as CO, CO_2 and H_2O [44], while part of them would contribute to the formation of unwanted organic by-products [45], such as

CH_3CH_2OH, CH_3OH, CH_4, HCOOH and HCHO in this work. In addition, no nitrogen monoxide (NO) was measured under all the experimental conditions, while NO_2 and N_2O were also detected.

Increasing the SED by changing the discharge power in a DBD reactor resulted in the increasing in the number of filaments in each discharge period [46], which was beneficial for the oxidation of ethyl acetate and its intermediates as more reaction channels were provided for the removal of ethyl acetate. As a consequence, the oxidation efficiency of ethyl acetate increases with increasing the SED.

In this single-stage plasma-catalytic process where the catalysts were placed in the discharge region and directly interacted with the plasma, besides the aforementioned gas phase reactions, plasma-assisted surface reactions in the catalyst bed also played a crucial role in determining the performance of the plasma-catalytic oxidation process as ethyl acetate, its intermediates and highly reactive species can be generated near the catalyst surface and participate surface reactions [47]. We have shown that the properties of the catalysts stheace adsorption sites for the aforementioned species. Generally, the number density of adsorption sites on a specific catalyst was in correlations with the S_{BET} of the catalyst. As shown in Table 1, the S_{BET} and average pore diameter of the nanofiber catalysts were much smaller compared to those of the bulk catalysts due to the plugging of the micro-pores of the nanofiber catalysts, especially for the nano-V_5Ti catalysts. Interestingly, the combination of the plasma with these nanofiber catalysts showed enhanced oxidation performance compared to the bulk catalysts. These results indicate the specific surface area and pore volume of the catalysts might not be the decisive factor affecting the reaction performance of the plasma-catalytic process. As confirmed by the XRD results, all the investigated catalysts showed the typical diffraction patterns of anatase TiO_2 together with weak diffraction peaks of rutile TiO_2. The crystalline size of these catalysts has strong links with the removal efficiency of ethyl acetate, carbon

balance and CO_2 selectivity of the plasma-catalytic reaction. Previous studies found that smaller crystalline size of a catalyst benefited the exposure of active sites on the catalyst surface, which in turn enhanced the reaction performance in VOC oxidation and NH_3-SCR of NO [48-49]. Tang et al. also reported smaller crystalline size could generate more surface defects and oxygen vacancies on the surface of Mn-Co catalysts, which were active for catalytic oxidation of VOC molecules [50].

The redox properties of the catalysts also played an important role in the plasma-catalytic oxidation reactions [51]. Previous studies reported the replacement of V^{5+} species into the lattice of TiO_2 over a series of V-Ti catalysts with the vanadium loading from 1% to 5% [52]. Considering the ion radius and valences of V^{5+} and Ti^{4+}, the formation of oxygen vacancies on the catalyst surface is expected at the interface of the vanadium and titanium species to maintain the electroneutrality. Oxygen vacancies act as the adsorption-desorption centers for the gas phase oxygen species and O radicals in catalytic oxidation of VOCs [53]. In this study, the presence of V^{4+} on the surface of V_5Ti catalysts indicates the formation of oxygen vacancies. The relative concentration $V^{4+}/(V^{4+}+V^{5+})$ in the nano-V_5Ti catalyst reached 30.3%, which was 32.9% higher than that of the bulk-V_5Ti catalyst. The abundant oxygen vacancies on the nano-V_5Ti catalyst could contribute to the enhancement of surface reactions for the oxidation of adsorbed ethyl acetate and its intermediates to final products of CO, CO_2 and H_2O. Previous studies of catalytic oxidation of formaldehyde showed that the formation of major byproducts, methyl formate, could be significantly inhibited over the nano-sized vanadium catalysts compared to the bulk samples [26, 54], while similar phenomena were observed in the catalytic oxidation of VOCs over vanadium-based nano-catalysts [34, 55].

Moreover, the V-O and Ti-O bonds could be prolonged and weakened in the V_5Ti catalysts considering the different ion radius of V^{5+} and Ti^{4+} [56]. The presence of redox pairs of V^{5+}/V^{4+} and Ti^{4+}/Ti^{3+} on the surface of the V_5Ti catalysts could accelerate the oxidation of

ethyl acetate through the enhanced electron transfer. This phenomenon could enhance the mobility of oxygen species and the generation of reactive oxygen species on the catalyst surface [57]. It is well established that O_{ads} was highly reactive in oxidation reactions due to its higher mobility compared to O_{lat}. The XPS spectra of O 1s showed the value of $O_{ads}/(O_{ads}+O_{lat})$ follows the sequence of nano-V_5Ti (15.4%) > bulk-V_5Ti (13.6%) > nano-TiO_2 (13.3%) > bulk-TiO_2 (10.5%). Higher relative concentration of O_{ads} on the surface of the nano-V_5Ti catalyst indicated that more oxygen species could be easily activated and participated in the plasma-catalytic oxidation of ethyl acetate with the help of surface reactions [58]. A good agreement between the reaction performance and the relative concentration of O_{ads} was observed in this work. The H_2-TPR profile of the catalysts showed that the reduction temperature of vanadium oxides significantly shifted to 359 °C in the nano-V_5Ti catalyst compared to that of the bulk-V_5Ti catalyst. This phenomenon was in line with the results of the XPS spectra of O 1s. Lower reduction temperature of the nano-V_5Ti catalyst indicated that the oxygen species on the surface of the nano-V_5Ti catalyst were much easier to be activated in the catalytic oxidation of ethyl acetate, which in turn enhances the surface oxidation of ethyl acetate, its intermediates and by-products in this work [51].

In addition, it is interesting to note that although the bulk-V_5Ti catalyst exhibited higher reducibility compared to the nano-TiO_2 catalyst, the reaction performance of these two catalysts were quite similar in terms of the removal efficiency, carbon balance and CO_2 selectivity. This might be attributed to the morphology and porosity of the catalysts. The SEM images showed a more compact structure of the bulk type catalysts, while the nanofibers interweaved into a porous network. Holzer et al. found that short-lived oxidizing species can be generated in the intra-particle volume of the catalysts [58], which could participate in the surface reactions in the presence of the catalysts. Guaitella et al. also reported the improved C_2H_2 oxidation in a plasma process combining Si-Ti catalysts with higher porosity [59]. They found

that the porous structure could facilitate the diffusion of the reactive oxygen species inside the catalyst layer and enhance the oxidation of the adsorbed pollutants and intermediates, which can be confirmed by the reduced formation of by-products using the coupling of the plasma with nanocatalysts.

4. Conclusions

In this work, the plasma-catalytic oxidation of ethyl acetate over V_2O_5/TiO_2 and TiO_2 catalysts was carried out in a coaxial DBD plasma reactor. The influence of nanofiber catalysts and bulk catalysts on the removal efficiency of ethyl acetate and CO_2 selectivity was compared and investigated with the case of using plasma alone. Significant enhancement in reaction performance of the plasma-catalytic oxidation process was observed when the using the V_2O_5/TiO_2 and TiO_2 nanofiber catalysts compared to the bulk catalysts, while the reaction performance followed the sequence of nano-V_5Ti > bulk V_5Ti > nano-TiO_2 > bulk TiO_2. The highest removal efficiency (96%) of ethyl acetate, carbon balance (99.3%) and CO_2 selectivity (55.6%) were achieved at the SED of 579.6 $J \cdot L^{-1}$ in the plasma-catalytic oxidation over the V_2O_5/TiO_2 nanofiber catalyst. A wide range of catalyst characterization techniques were used to understand the effect of catalyst properties on the reaction performance of the plasma-catalytic oxidation process. The morphology and structure of the nanofiber catalysts were confirmed using SEM, TEM and XRD, showing the V_2O_5/TiO_2 nanofiber catalysts had smaller crystalline size compared to the bulk catalysts. The V_2O_5/TiO_2 nanofiber catalysts also showed much higher relative concentration of surface adsorbed oxygen (O_{ads}) species compared to the corresponding bulk catalysts, which play a key role in the oxidation of ethyl acetate and its intermediates on the catalyst surface. The formation of more reduced vanadium species (V^{4+}) in the nano-V_5Ti catalysts compared to the bulk-V_5Ti catalysts indicated the formation of more oxygen vacancies on the surface of the nano-V_5Ti catalysts, which is in line

with the results of O_{ads}. The reducibility of the V_2O_5/TiO_2 nanofiber catalysts was also improved considering the lower reduction temperature of the nano-V_5Ti catalysts compared to the bulk-V_5Ti catalysts, which suggested the facility of activations of surface oxygen species in the plasma region and contributed to the plasma-catalytic oxidation reactions.

Acknowledgements

This work is financially supported by National Natural Science Foundation of China (No. 51606166), Ningbo Natural Science Foundation and K.C. Wong Magna Fund in Ningbo University.

References

(1) Koppmann, R., *Volatile organic compounds in the atmosphere*. Blackwell Publishing Ltd.: Oxford, UK, 2007.

(2) Vandenbroucke, A. M.; Morent, R.; De Geyter, N.; Leys, C., Non-thermal plasmas for non-catalytic and catalytic VOC abatement. *J. Hazard. Mater.* **2011,** *195*, 30-54.

(3) Bo, Z.; Yan, J. H.; Li, X. D.; Chi, Y.; Cen, K. F., Simultaneous removal of ethyl acetate, benzene and toluene with gliding arc gas discharge. *J. Zhejiang Univ.-Sci. A* **2008,** *9* (5), 695-701.

(4) Whitehead, J. C., Plasma-catalysis: the known knowns, the known unknowns and the unknown unknowns. *J. Phys. D: Appl. Phys.* **2016,** *49*, 243001.

(5) Neyts, E. C.; Ostrikov, K. K.; Sunkara, M. K.; Bogaerts, A., Plasma catalysis: Synergistic effects at the nanoscale. *Chem. Rev.* **2015,** *115* (24), 13408-46.

(6) Zhu, X.; Liu, S.; Cai, Y.; Gao, X.; Zhou, J.; Zheng, C.; Tu, X., Post-plasma catalytic removal of methanol over Mn-Ce catalysts in an atmospheric dielectric barrier discharge. *Appl. Catal. B: Environ.* **2016,** *183*, 124-132.

(7) Ojala, S.; Pitkäaho, S.; Laitinen, T.; Niskala Koivikko, N.; Brahmi, R.; Gaálová, J.; Matejova, L.; Kucherov, A.; Päivärinta, S.; Hirschmann, C.; Nevanperä, T.; Riihimäki, M.; Pirilä, M.; Keiski, R. L., Catalysis in VOC abatement. *Topics in Catal.* **2011,** *54* (16-18), 1224-1256.

(8) Chen, T.; Rodionov, V. O., Controllable catalysis with nanoparticles: Bimetallic alloy

systems and surface adsorbates. *ACS Catal.* **2016**, 4025-4033.
(9) Montini, T.; Melchionna, M.; Monai, M.; Fornasiero, P., Fundamentals and catalytic applications of CeO_2-based materials. *Chem. Rev.* **2016**.
(10) Tsoncheva, T.; Ivanova, L.; Rosenholm, J.; Linden, M., Cobalt oxide species supported on SBA-15, KIT-5 and KIT-6 mesoporous silicas for ethyl acetate total oxidation. *Appl. Catal. B: Environ.* **2009,** *89* (3-4), 365-374.
(11) Gandhe, A. R.; Rebello, J. S.; Figueiredo, J. L.; Fernandes, J. B., Manganese oxide OMS-2 as an effective catalyst for total oxidation of ethyl acetate. *Appl. Catal. B: Environ.* **2007,** *72* (1-2), 129-135.
(12) Japke, E.; Casapu, M.; Trouillet, V.; Deutschmann, O.; Grunwaldt, J. D., Soot and hydrocarbon oxidation over vanadia-based SCR catalysts. *Catal. Today* **2015,** *258*, 461-469.
(13) Gannoun, C.; Delaigle, R.; Debecker, D. P.; Eloy, P.; Ghorbel, A.; Gaigneaux, E. M., Effect of support on V_2O_5 catalytic activity in chlorobenzene oxidation. *Appl. Catal. A: Gene.* **2012,** *447-448*, 1-6.
(14) Barakat, T.; Rooke, J. C.; Franco, M.; Cousin, R.; Lamonier, J.-F.; Giraudon, J.-M.; Su, B.-L.; Siffert, S., Pd- and/or Au-loaded Nb- and V-doped macro-mesoporous TiO_2 supports as catalysts for the total oxidation of VOCs. *Euro. J. Inorg. Chem.* **2012,** *2012* (16), 2812-2818.
(15) Kumar, S. Gas phase oxidation of dimethyl sulfide by titanium dioxide based catalysts. Miami University, Miami, 2004.
(16) Sahle-Demessie, E.; Devulapelli, V. G., Vapor phase oxidation of dimethyl sulfide with ozone over V_2O_5/TiO_2 catalyst. *Appl. Catal. B: Environ.* **2008,** *84* (3-4), 408-419.
(17) Debecker, D. P.; Bouchmella, K.; Delaigle, R.; Eloy, P.; Poleunis, C.; Bertrand, P.; Gaigneaux, E. M.; Mutin, P. H., One-step non-hydrolytic sol-gel preparation of efficient V_2O_5-TiO_2 catalysts for VOC total oxidation. *Appl. Catal. B: Environ.* **2010,** *94* (1-2), 38-45.
(18) Yu, M. F.; Lin, X. Q.; Li, X. D.; Yan, M.; Prabowo, B.; Li, W. W.; Chen, T.; Yan, J. H., Catalytic destruction of PCDD/Fs over vanadium oxide-based catalysts. *Environ. Sci. Pollut. Res. Inter.* **2016**.
(19) Zhang, Z.; Jiang, Z.; Shangguan, W., Low-temperature catalysis for VOCs removal in technology and application: A state-of-the-art review. *Catal. Today* **2016,** *264*, 270-278.
(20) Oda, T.; Yamaji, K.; Takahashi, T., Decomposition of dilute trichloroethylene by nonthermal plasma processing - Gas flow rate, catalyst, and ozone effect. *IEEE Trans. Ind. Appl.* **2004,** *40* (2), 430-436.
(21) Chae, J. O.; Demidiouk, V.; Yeulash, M.; Choi, I. C.; Jung, T. G., Experimental study for indoor air control by plasma-catalyst hybrid system. *IEEE Trans. Plasma Sci.* **2004,** *32* (2),

493-497.
(22) Kim, H.-H.; Lee, Y.-H.; Ogata, A.; Futamura, S., Plasma-driven catalyst processing packed with photocatalyst for gas-phase benzene decomposition. *Catal. Commun.* **2003,** *4* (7), 347-351.
(23) Oda, T.; Takahashi, T.; Kohzuma, S., Decomposition of dilute trichloroethylene by using nonthermal plasma processing-frequency and catalyst effects. *IEEE Trans. Ind. Appl.* **2001,** *37* (4), 965-970.
(24) Zhu, X.; Yang, Y.; Geng, X.; Zheng, C.; Zhou, J.; Gao, X.; Luo, Z.; Ni, M.; Cen, K., Catalytic oxidation of dimethyl sulfide over commercial V-W/Ti catalysts: Plasma activation at low temperatures. *IEEE Trans. Plasma Sci.* **2016**.
(25) Wang, F.; Dai, H.; Deng, J.; Bai, G.; Ji, K.; Liu, Y., Manganese oxides with rod-, wire-, tube-, and flower-like morphologies: highly effective catalysts for the removal of toluene. *Environ. Sci. & Technol.* **2012,** *46* (7), 4034-41.
(26) Bhattacharyya, K.; Varma, S.; Tripathi, A. K.; Bharadwaj, S. R.; Tyagi, A. K., Mechanistic insight by in situ FTIR for the gas phase photo-oxidation of ethylene by V-doped titania and nano titania. *J. Phys. Chem. B* **2009,** *113* (17), 5917-28.
(27) Hosseini, S. A.; Salari, D.; Niaei, A.; Deganello, F.; Pantaleo, G.; Hojati, P., Chemical-physical properties of spinel $CoMn_2O_4$ nano-powders and catalytic activity in the 2-propanol and toluene combustion: Effect of the preparation method. *J. Environ. Sci. Health. Part a, Toxic/hazard. Sub. & environ. Eng.* **2011,** *46* (3), 291-7.
(28) Bianchi, C. L.; Gatto, S.; Pirola, C.; Naldoni, A.; Di Michele, A.; Cerrato, G.; Crocellà, V.; Capucci, V., Photocatalytic degradation of acetone, acetaldehyde and toluene in gas-phase: Comparison between nano and micro-sized TiO_2. *Appl. Catal. B: Environ.* **2014,** *146*, 123-130.
(29) Sanjeeva Gandhi, M.; Mok, Y. S., Shape-dependent plasma-catalytic activity of ZnO nanomaterials coated on porous ceramic membrane for oxidation of butane. *Chemosphere* **2014,** *117C*, 440-446.
(30) Zhu, T.; Li, J.; Jin, Y. Q.; Liang, Y. H.; Ma, G. D., Gaseous phase benzene decomposition by non-thermal plasma coupled with nano titania catalyst. *Inter. J. Environ. Sci. Technol.* **2009,** *6* (1), 141-148.
(31) Jia, Z. X.; Vega-Gonzalez, A.; Ben Amar, M.; Hassouni, K.; Tieng, S. T.; Touchard, S.; Kanaev, A.; Duten, X., Acetaldehyde removal using a diphasic process coupling a silver-based nano-structured catalyst and a plasma at atmospheric pressure. *Catal. Today* **2013,** *208*, 82-89.
(32) Zhang, Y.-R.; Van Laer, K.; Neyts, E. C.; Bogaerts, A., Can plasma be formed in catalyst pores? A modeling investigation. *Appl. Catal. B: Environ.* **2016,** *185*, 56-67.

(33) Van Laer, K.; Bogaerts, A., Fluid modelling of a packed bed dielectric barrier discharge plasma reactor. *Plasma Sour. Sci. Technol.* **2016,** *25* (1), 015002.

(34) Zhu, X.; Chen, J.; Yu, X.; Zhu, X.; Gao, X.; Cen, K., Controllable synthesis of novel hierarchical V_2O_5/TiO_2 nanofibers with improved acetone oxidation performance. *RSC Adv.* **2015,** *5* (39), 30416-30424.

(35) Zhu, X.; Tu, X.; Mei, D.; Zheng, C.; Zhou, J.; Gao, X.; Luo, Z.; Ni, M.; Cen, K., Investigation of hybrid plasma-catalytic removal of acetone over CuO/γ -Al_2O_3 catalysts using response surface method. *Chemosphere* **2016,** *155*, 9-17.

(36) Sing, K. S., Reporting physisorption data for gas/solid systems with special reference to the determination of surface area and porosity (Recommendations 1984). *Pure Appl. Chem.* **1985,** *57* (4), 603-619.

(37) Zakaria, Z. Y.; Linnekoski, J.; Amin, N. A. S., Catalyst screening for conversion of glycerol to light olefins. *Chem. Eng. J.* **2012,** *207*, 803-813.

(38) Liu, F.; He, H.; Xie, L., XAFS Study on the Specific Deoxidation behavior of iron titanate catalyst for the selective catalytic reduction of NO_x with NH_3. *ChemCatChem* **2013,** *5* (12), 3760-3769.

(39) Ji, P.; Gao, X.; Du, X.; Zheng, C.; Luo, Z.; Cen, K., Relationship between the molecular structure of V_2O_5/TiO_2 catalysts and the reactivity of SO_2 oxidation. *Catal. Sci. Technol.* **2016,** *6* (4), 1187-1194.

(40) Mei, D.; Zhu, X.; Wu, C.; Ashford, B.; Williams, P. T.; Tu, X., Plasma-photocatalytic conversion of CO_2 at low temperatures: Understanding the synergistic effect of plasma-catalysis. *Appl. Catal. B: Environ.* **2016,** *182*, 525-532.

(41) Zhu, X.; Gao, X.; Zheng, C.; Wang, Z.; Ni, M.; Tu, X., Plasma-catalytic removal of a low concentration of acetone in humid conditions. *RSC Adv.* **2014,** *4* (71), 37796-37805.

(42) Fisher, E. M.; Pitz, W. J.; Curran, H. J.; Westbrook, C. K., Detailed chemical kinetic mechanisms for combustion of oxygenated fuels. *Proceed. Combust. Inst.* **2000,** *28* (2), 1579-1586.

(43) El-Nahas, A. M.; Navarro, M. V.; Simmie, J. M.; Bozzelli, J. W.; Curran, H. J.; Dooley, S.; Metcalfe, W., Enthalpies of Formation, Bond Dissociation Energies and Reaction Paths for the Decomposition of Model Biofuels: Ethyl Propanoate and Methyl Butanoate. *J. Phys. Chem. A* **2007,** *111* (19), 3727-3739.

(44) Fridman, A. A., *Plasma chemistry*. Cambridge University Press: 2008.

(45) Zhu, X.; Zhang, S.; Yang, Y.; Zheng, C.; Zhou, J.; Gao, X.; Tu, X., Enhanced performance for plasma-catalytic oxidation of ethyl acetate over $La_{1-x}Ce_xCoO_{3+\delta}$ catalysts. *Appl. Catal. B:*

Environ. **2017,** *213*, 97-105.

(46) Mei, D.; He, Y.-L.; Liu, S.; Yan, J.; Tu, X., Optimization of CO_2 conversion in a cylindrical dielectric barrier discharge reactor using design of experiments. *Plasma Process Polym.* **2016,** *13* (5), 544-556.

(47) Lin, H.; Huang, Z.; Shangguan, W. F.; Peng, X. S., Temperature-programmed oxidation of diesel particulate matter in a hybrid catalysis-plasma reactor. *Proceed. Combust. Inst.* **2007,** *31*, 3335-3342.

(48) Saqer, S. M.; Kondarides, D. I.; Verykios, X. E., Catalytic oxidation of toluene over binary mixtures of copper, manganese and cerium oxides supported on γ-Al_2O_3. *Appl. Catal. B: Environ.* **2011,** *103* (3-4), 275-286.

(49) Wu, G.; Li, J.; Fang, Z.; Lan, L.; Wang, R.; Lin, T.; Gong, M.; Chen, Y., Effectively enhance catalytic performance by adjusting pH during the synthesis of active components over $FeVO_4/TiO_2$–WO_3–SiO_2 monolith catalysts. *Chem. Eng. J.* **2015,** *271*, 1-13.

(50) Tang, W.; Wu, X.; Li, S.; Li, W.; Chen, Y., Porous Mn-Co mixed oxide nanorod as a novel catalyst with enhanced catalytic activity for removal of VOCs. *Catal. Commun.* **2014,** *56*, 134-138.

(51) Zhu, X.; Gao, X.; Yu, X.; Zheng, C.; Tu, X., Catalyst screening for acetone removal in a single-stage plasma-catalysis system. *Catal. Today* **2015,** *256*, 108-114.

(52) Wu, D.; Tong, H.; Chen, Q.; Xia, C., Photocatalytic water splitting into O_2 over vanadium doped nano rutile TiO_2. *Integ. Ferro.* **2011,** *127* (1), 55-62.

(53) Roxana Morales, M.; Agueero, F. N.; Cadus, L. E., Catalytic Combustion of n-Hexane Over Alumina Supported Mn-Cu-Ce Catalysts. *Catal. Lett.* **2013,** *143* (10), 1003-1011.

(54) Popova, G. Y.; Andrushkevich, T. V. Z., G.A., Heterogeneous selective oxidation of formaldehyde over oxide catalysts. 2. Catalytic properties of V-Ti-oxide catalysts. *Kinetika i Kataliz* **1997,** *38* (2), 285-288.

(55) Yu, M. F.; Li, W. W.; Li, X. D.; Lin, X. Q.; Chen, T.; Yan, J. H., Development of new transition metal oxide catalysts for the destruction of PCDD/Fs. *Chemosphere* **2016,** *156*, 383-391.

(56) Shannon, R. D., Revised effective ionic radii and systematic studies of interatomic distances in halides and chalcogenides. *Acta Crystal. Sec. A* **1976,** *32* (5), 751-767.

(57) Avdeev, V. I.; Tapilin, V. M., Electronic Structure and Stability of Peroxide Divanadate Species V(O−O) on the TiO_2 (0 0 1) Surface Reconstructed. *J. Phys. Chem. C* **2009,** *113* (33), 14941-14945.

(58) Holzer, F., Combination of non-thermal plasma and heterogeneous catalysis for oxidation

of volatile organic compounds Part 1. Accessibility of the intra-particle volume. *Appl. Catal. B: Environ.* **2002,** *38* (3), 163-181.

(59) Guaitella, O.; Thevenet, F.; Puzenat, E.; Guillard, C.; Rousseau, A., C_2H_2 oxidation by plasma/TiO_2 combination: Influence of the porosity, and photocatalytic mechanisms under plasma exposure. *Appl. Catal. B: Environ.* **2008,** *80* (3-4), 296-305.